

# CALIBRATION OF THE FAST 12-CHANNEL ECE SPECTROMETER AT JET

by

R.M. Niestadt, B.J.D. Tubbing, Th. Oyevaar

Rijnhuizen Report 86-168

## CONTENTS

	<u>page</u>
Abstract	1
1. Introduction	2
2. Description of the spectrometer	3
2.1 Introduction	3
2.2 The 12-channel polychromator	3
2.3 Detectors, cryostats and signal conditioning	7
3. Characteristics of the spectrometer	8
3.1 Dispersion	8
3.2 Resolution	10
3.3 Stray radiation	12
3.4 Polarisation dependence	14
3.5 Different entrance slits	17
4. Antenna pattern measurements	19
4.1 Introduction	19
4.2 Patterns of several components	20
5. Absolute calibration of the polychromator	27
5.1 Introduction	27
5.2 Large area black body source	27
5.3 Cross-calibration	28
5.4 Antenna pattern integrations	28
5.5 Mode scrambler	29
6. Conclusions and discussion	32
References	33

CALIBRATION OF THE FAST 12-CHANNEL  
ECE SPECTROMETER AT JET

by

R.M. Niestadt\*, B.J.D. Tubbing, Th. Oyevaar  
Association Euratom-FOM  
FOM-Instituut voor Plasmafysica  
Rijnhuizen, Nieuwegein, The Netherlands

ABSTRACT

Measurements on the 12-channel ECE grating polychromator at the Joint European Torus are reported. This report describes the performance of the spectrometer in terms of sensitivity and spectral resolution. Measures to improve the systems responsivity and to overcome some characteristic problems of the spectrometer are reported. In addition, a comparison between different methods of absolute calibration of the system is presented.

\* Present address: ASM Europe B.V., Bilthoven.

## 1. INTRODUCTION

This report describes the calibration of the ECE 12-channel polychromator at the Joint European Torus. The main objectives of this diagnostic are:

- The investigation of MHD and sawtooth activity. Use of the 12-channel spectrometer will enable rapid oscillations in the electron temperature profile to be studied. This should provide detailed information on the space location of such oscillations. Also the influence of the electron temperature profile on the stability to resistive tearing modes may be studied.
- Localisation of the inversion and mixing radii as well as the electron heat conductivity profile can be inferred from sawtooth analysis.
- The study of the effects of additional heating (ICRH, neutral particle injection) on the electron temperature profile; it may be possible to determine the spatial energy deposition.
- The investigation of thermal transport and energy confinement during pellet injection. Rapid redistribution of thermal energy occurs on a millisecond timescale; the high time resolution of this polychromator enables detailed studies of these phenomena.
- Analysis of the composition of the electron velocity distribution function. Determination of the energy of superthermal components might be inferred from the sensitivity of ECE to a non-maxwellian energy distribution, and by using special computer codes.

These objectives can be achieved due to the characteristics of this ECE spectrometer:

- The 12-channel grating polychromator is particularly suited to observe phenomena on a timescale of microseconds.
- The spectral resolution of the spectrometer is proportional to the wavelength of the received radiation, resulting in a radial spatial resolution which is nearly constant (5-7 cm) over the entire JET plasma.
- The responsivity of the system is typical 3.5 eV/ $\mu$ V at system entrance, deteriorating to 70 eV/ $\mu$ V after connection with the JET waveguide. This results in a signal to noise ratio of about 150 at 20 kHz electrical bandwidth and the spectrometer tuned to receive radiation from the plasma centre at  $f = 190$  GHz.

## 2. DESCRIPTION OF THE SPECTROMETER

### 2.1 Introduction

In 1980 a grating polychromator was proposed [1] to measure Electron Cyclotron Emission in the Joint European Torus fusion plasma experiment, as a diagnostic for the electron temperature. There are several methods to measure ECE radiation: interferometric (Michelson and Fabry-Pérot interferometers), superheterodyne techniques and grating polychromators, which are all described in Ref. [2].

Grating polychromators have the great advantage that, simultaneously, all channels can be sampled on a high sample rate up to 500 kHz. Because of the high spectral resolution of the instrument this results, together with the typical  $1/R$  dependence of the tokamak magnetic field, in a constant high radial spatial resolution. For conventional grating polychromators, the frequency range covered ( $f_{\max}/f_{\min}$ ) with one grating is typically  $\leq 1.5$ . This means that for a tokamak plasma, where the frequency range in one harmonic is usually greater than the above value, one always has to employ several gratings for one harmonic to be studied\*. In the grating polychromator described here, the principle of conical diffraction is used. The main difference with conventional grating spectrometers is that the grating is rotated on an axis perpendicular to the grooves instead of parallel to the grooves. This has the practical result of a larger frequency range that can be covered with one grating ( $f_{\max}/f_{\min} \approx 5$ ). Secondly, conical diffraction ensures the blaze condition to be maintained during rotation of the grating, resulting in an efficiency which is independent of the grating angle and thus almost constant for the whole frequency range. For a full description of the conical diffraction principle and the derivation of the grating equation see Ref. [3].

### 2.2 The 12-channel polychromator

In Fig. 2.2.1 a schematic view of the polychromator is shown. The grating is used in a Littrow setting mounted in cat's eye with a plane mirror.

---

\* (This is only true for the first two harmonics; the frequency range that can be viewed without harmonic overlap is  $\ell+1/\ell$ , with  $\ell$  the harmonic number).

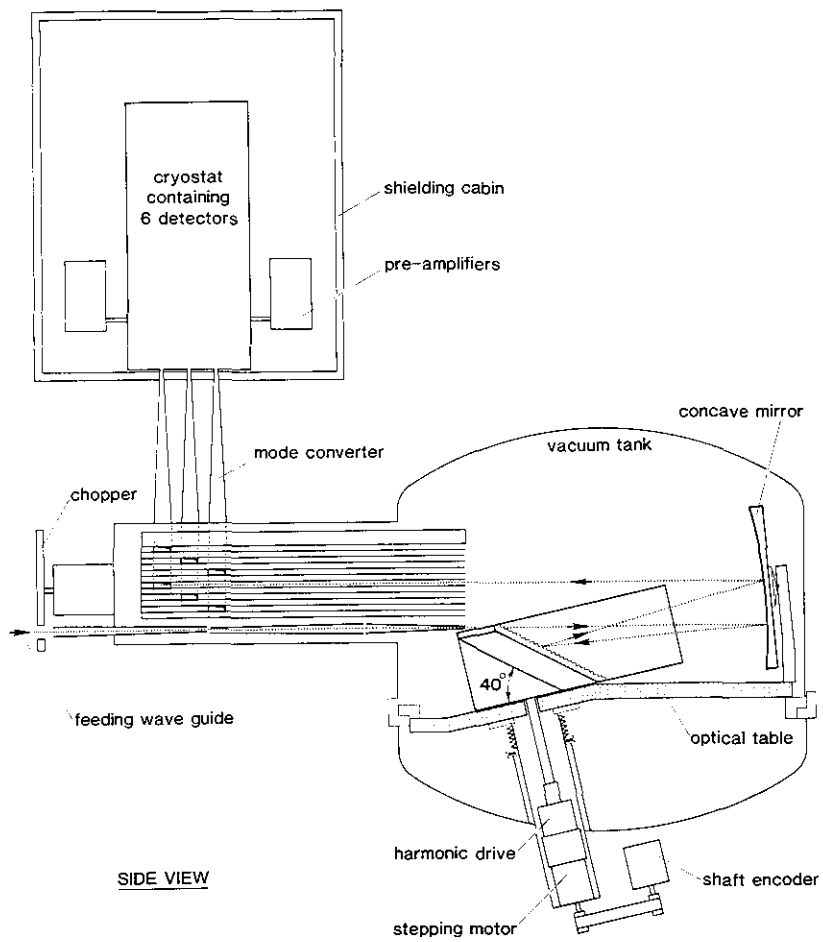
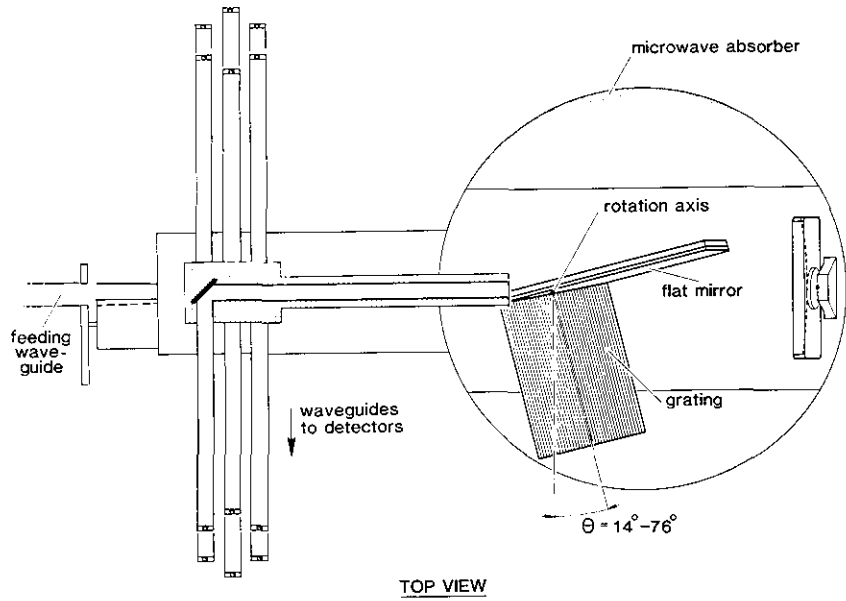


Fig. 2.2.1. Top view and side view of the 12-channel ECE polychromator as installed at JET.

The ECE radiation from the JET plasma is transmitted by an overmoded millimetre waveguide/antenna system. The spectrometer is fed by a S-band (dimensions  $72.14 \times 34.04$  mm) waveguide. The incoming radiation first passes a number of unidirectional low-pass grating filters [4] and then a high-pass Timusk filter [5]. Between these two kinds of filters the waveguide is tapered down from S-band to  $40.4 \times 20.2$  mm. After the highpass radiation filter the waveguide tapers down to the chopper aperture of  $40.4 \times 10.1$  mm\*. The chopper is included to be able to correct for any possible baseline drift. After tapering back to  $40.4 \times 20.2$  mm the radiation is next guided to the entrance slit of the spectrometer itself.

The spectral image of the entrance aperture is strongly deformed by the diffraction of the grating; it will be rotated with respect to its orientation before diffraction. Since this rotation is completely defined for each grating angle, one can orient the spectral image of the entrance aperture in any chosen direction by presetting the angle of the entrance slit. To realise this, a mode converter is incorporated which transforms the  $40.4 \times 20.2$  mm waveguide to one with a 15 mm circular diameter. To reach the entrance aperture of  $40.0 \times 13.5$  mm in principle the inverse procedure has to be followed. Therefore a rotating section consisting of a short piece of circular waveguide and two mode converters are applied in the waveguide system leading to the entrance aperture. Although the radiation incident to the spectrometer will be largely in the  $TE_{10}$  mode, the mode structure in the entrance waveguide will be rather complicated due to the rotation. The design and manufacturing of these waveguide mode converters from the  $TE_{10}$  mode in oversized rectangular to the  $TE_{11}$  mode in oversized circular waveguide is fully described in Ref. [6]. A detailed view of the rotating section in the entrance waveguide is shown in Fig. 2.2.2.

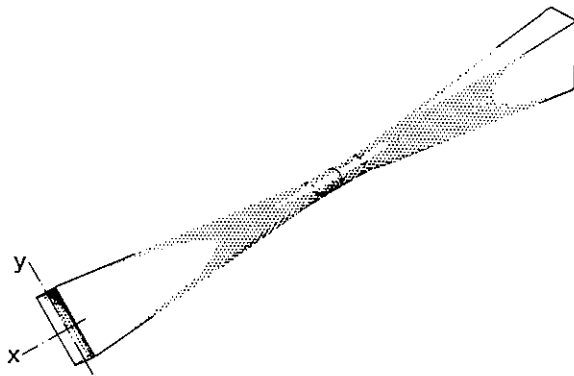


Fig. 2.2.2.

The rotating section in the entrance waveguide.

\* This tapering has been employed to enhance the duty cycle of the chopper.

The entrance slit is in the focal plane of a concave mirror, which reflects the incident radiation onto the grating. The dispersion is perpendicular to the grooves and because the plane mirror is mounted flush to the grating, the diffracted radiation is reflected back to the concave mirror which now focusses the radiation on the exit apertures. As the spectral image is located on the surface of a cone with a half top-angle of  $(90-\gamma)$  where  $\gamma$  is the grating angle, the image plane deviates from a straight line for the upper channels for large grating angles. To accommodate for this effect when observing high frequencies, the apertures of the upper four exit waveguides are extended in the horizontal direction (see Fig. 2.2.3). These four upper exit apertures are tapered down smoothly to measure  $40.0 \times 13.5$  mm, the same size as the other exit waveguides. Then the even-numbered channels are diverted to one cryostat and the odd-numbered channels to the other. As the radiation has to be coupled into twelve detectors contained in cryostats with  $\emptyset$  15 mm entrance apertures, again a converter is required to perform the conversion from rectangular to circular waveguide for each channel.

As an example, the ray trace from the entrance waveguide to the upper waveguide is shown in Fig. 2.2.3.

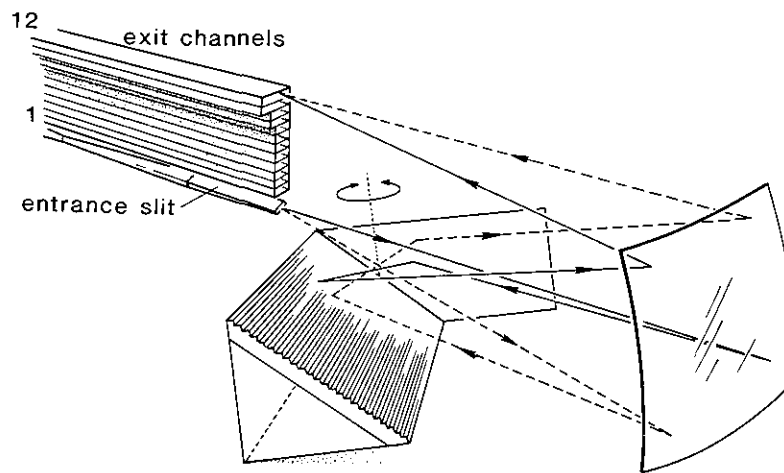


Fig. 2.2.3. Ray traces in the spectrometer.

### 2.3 Detectors, cryostats and signal conditioning

The detectors are liquid helium-cooled InSb bolometers, manufactured by QMC Ltd. These detectors are broad-banded (0.01-600 kHz), have a high responsivity (typical 2 kV/W) and possess low noise characteristics (typical 2.4 nV/√Hz). The detectors are followed by pre-amplifiers (also from QMC) which do not distort the low noise qualities of the detectors: voltage and current noise are comparable with the detector noise. The gain of these pre-amplifiers is selectable from 40-60-80 dB. The twelve detectors are mounted into two cryostats which, together with the pre-amplifiers, are housed in screening boxes which are covered inside with mu-metal to avoid penetration of stationary, low magnetic fields. The cryostats have a holdtime of 200 hours for 6.5 litre of liquid helium.

The signals of the pre-amplifiers are fed into a modular and programmable signal conditioning system (SICOS), consisting of high-pass, low-pass and precision amplifiers.

Then the system is interfaced with three 4-channel 1 MHz A/D converters with compatible memory to record the output of the twelve channels on a microsecond timescale. In parallel, six slow channels can be assigned to be stored in a 6-channel 20 kHz A/D converter to observe plasma fluctuations on a longer timebase. Data acquisition will be done on the NORD 100 and NORD 500 computers at JET. The complete signal diagram is shown in Fig. 2.3.1.

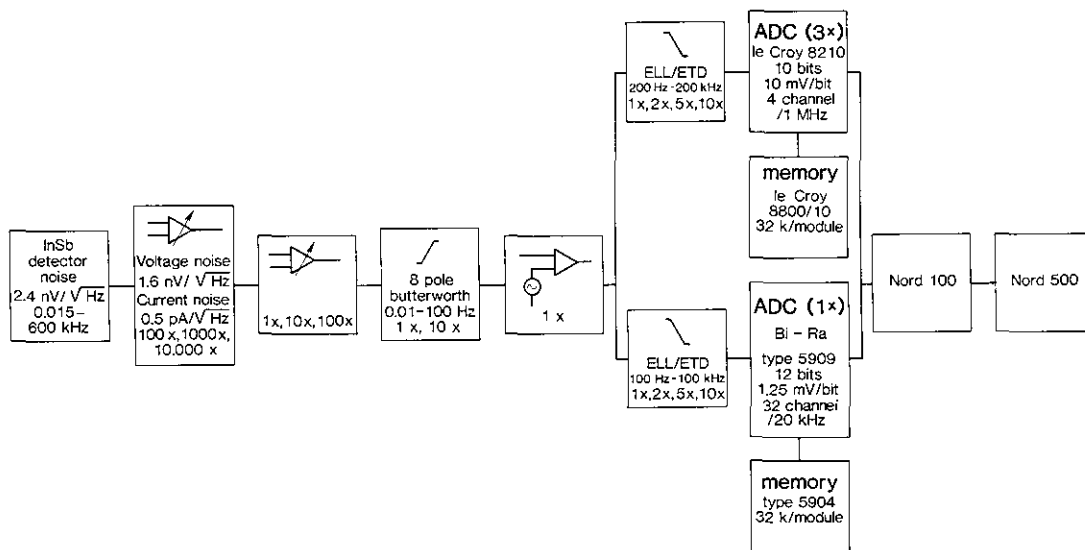


Fig. 2.3.1. Signal diagram and data acquisition at JET.

### 3. CHARACTERISTICS OF THE SPECTROMETER

#### 3.1 Dispersion

The grating equation, in the conventionally used coordinate system (as defined in Fig. 3.1.1 and Fig. 3.1.2), reads:

$$\sin \phi + \sin \phi' = \frac{m\lambda}{g \cos \gamma} \quad (3.1.1)$$

where  $\phi$  is related to the entrance angle,  $\phi'$  to the exit angle and  $\gamma$  to the grating angle. The parameter  $g$  is defined as the grating constant and  $\phi_B = 50^\circ$  is the blaze angle. For a full definition of the several angles used to describe the conical diffraction principle, see Ref. [3]. The geometry of the spectrometer fixes the angles  $\phi$  and  $\gamma$ , whereas the exit angles  $\phi'$  are determined by the position of the exit apertures. The polychromator is equipped with twelve exit waveguides, for which the blaze condition,  $\phi_B = \frac{1}{2}(\phi + \phi')$ , is accomplished for a location exactly between exits 6 and 7.

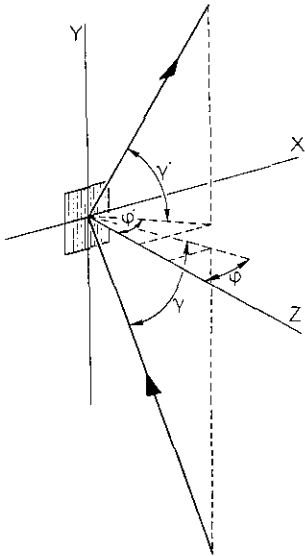


Fig. 3.1.1.

Definition of the conventional system.

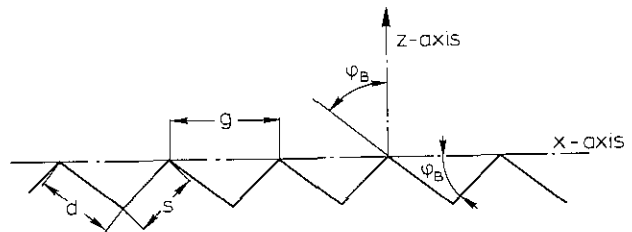


Fig. 3.1.2.

Definition of the grating constant and the blaze angle.

The dispersion curves are measured using a variable frequency source (Backward Wave Oscillator 100-170 GHz) and a mode scrambler. The scrambler ensures all possible standing wave structures between the source and the detector to be suppressed. On top of this, a small

amount of frequency modulation of the source (small compared to the spectral resolution of the polychromator) is applied. With the aid of a small PDP 11/23 computer the grating is rotated (by steps of  $0.1^\circ$ ) and the output voltage of all twelve detectors is registered as a function of the grating angle  $\vartheta$  and stored in a data file for further analysis. An example of such a measurement at a single frequency on a grating with grating constant  $g = 1.8 \text{ mm}$  is shown in Fig. 3.1.3.

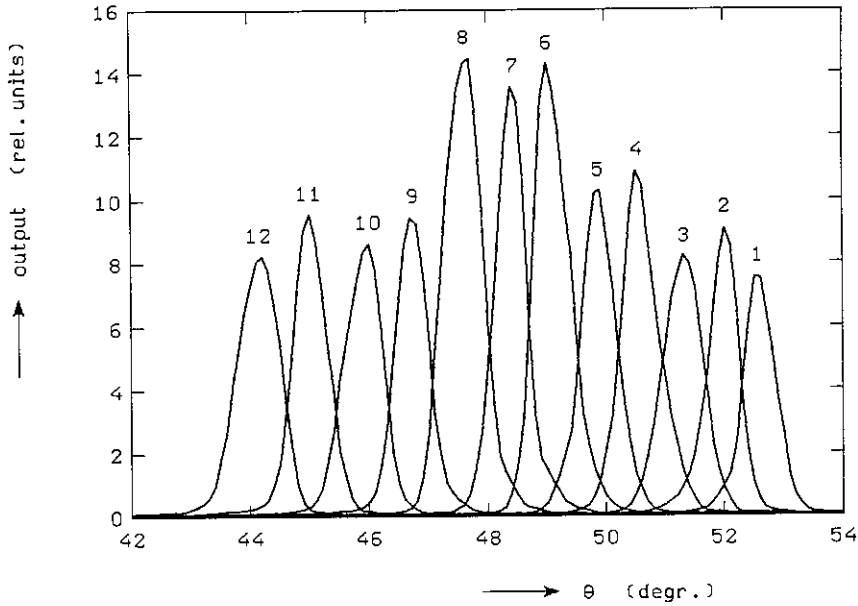


Fig. 3.1.3. The 12 instrument functions obtained from a grating scan ( $42 < \vartheta < 54$ ) at  $f = 165 \text{ GHz}$ .

From these measurements, the dispersion curves are calculated using 26 different frequencies (stepsize is 2.5 GHz). The points at  $f > 170 \text{ GHz}$  are measured with a  $g = 3.6 \text{ mm}$  grating, using second order dispersion. The grating angle for which a channel yields the maximum response, is calculated by means of a weighted average:

$$\langle \vartheta (f) \rangle_i = \frac{\int_{\vartheta_{\min}}^{\vartheta_{\max}} \vartheta V_{\text{det}}(f), i d \vartheta}{\int_{\vartheta_{\min}}^{\vartheta_{\max}} V_{\text{det}}(f), i d \vartheta}, \quad (3.1.2)$$

where  $\vartheta_{\min}$ ,  $\vartheta_{\max}$  are the begin and end values of the grating scan;  $i = 1, 12$ . This procedure corrects for the fact that the response might not be completely gaussian.

The dispersion curves for the  $g = 1.8$  mm grating are shown in Fig. 3.1.4; when the  $g = 3.6$  mm grating is mounted in the spectrometer (in use when JET's magnetic field  $\leq 2.6$  T), simply divide the frequency scale by a factor 2.

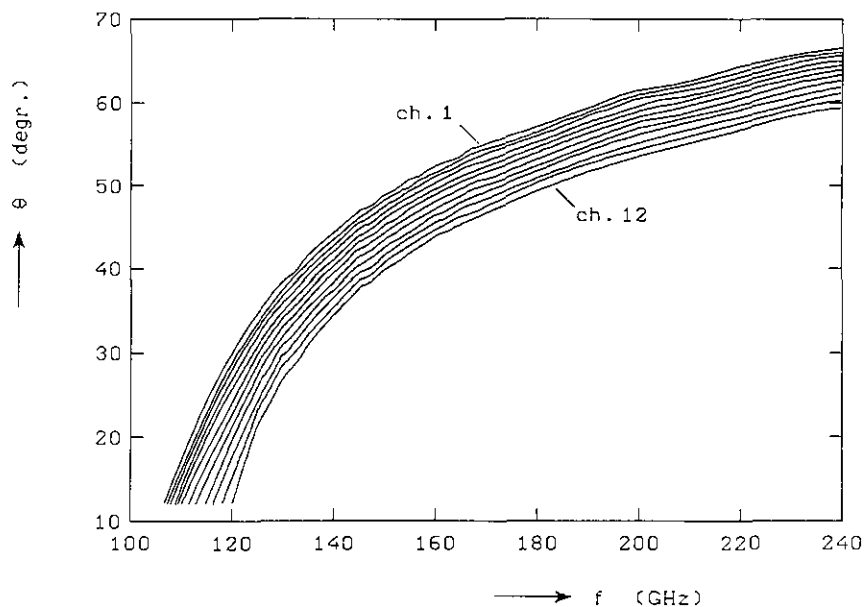


Fig. 3.1.4. The dispersion curves for the  $g = 1.8$  mm grating.

### 3.2 Resolution

The resolutions of all channels of the polychromator as a function of frequency are calculated from the measurements described in the preceding section. From Fig. 3.1.3,  $\Delta\theta$  values are determined as the FWHM (Full Width Half Maximum) of the twelve different instrument functions. With the dispersion curves, as shown in Fig. 3.1.4,  $\Delta\theta$  values are converted to  $\Delta f$  values. The resolution is defined as  $R = f/\Delta f$ . In general,  $\Delta f$  is of the order of 1.3 GHz ( $f = 115$  GHz) up to 4.0 GHz ( $f = 170$  GHz). The resolution averaged over all channels as a function of frequency is shown in Fig. 3.2.1.

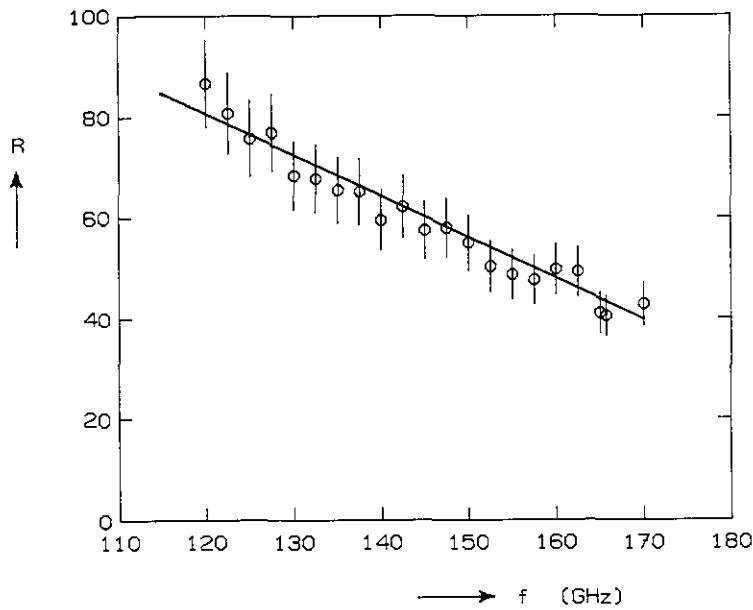
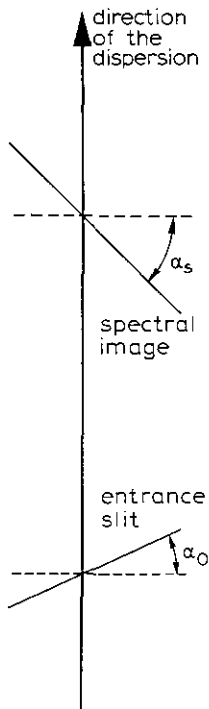


Fig. 3.2.1. Average resolution vs frequency.

The resolution is very much dependent on the preset angle  $\alpha_0$  of the entrance slit. Optimal resolution will only be achieved for an optimal image of the entrance slit on the exit waveguides, i.e. the slit angle which produces the smallest width of this spectral image in the direction of the dispersion. An expression for the orientation of the spectral image is derived in Ref. [3]:

$$\tan \alpha_s = \frac{(\sin \phi + \sin \phi') \sin \gamma}{\cos \phi'} - \frac{\cos \phi}{\cos \phi'} \tan \alpha_0, \quad (3.2.1)$$



where  $\alpha_s$  is the angle between the spectral slit image and the direction perpendicular to the dispersion (Fig. 3.2.2). This expression has been experimentally verified.

In general practice,  $\alpha_0$  is set as to give an optimal spectral slit image ( $\alpha_s = 0$ ) for the blaze position, i.e. half-way between channel 6 and channel 7. This setting is done automatically whenever the grating angle is changed. In this manner, the deviation of  $\alpha_s$  from zero is equally distributed over the upper and lower channels.

Fig. 3.2.2.

Definition of the angles  $\alpha_s$  and  $\alpha_0$ .

As an example, the deviation for  $\gamma = 14^\circ$  is  $\leq 1.5^\circ$  for the extreme channels; for  $\gamma = 60^\circ$  this increases to  $\leq 12^\circ$ .

It has been found that there exists no dependence of the resolution figures on the incoming polarisation (within experimental errors). Because a "shielding wing" has been fitted in the spectrometer (see section 3.3) the resolution has been slightly decreased to 85% of its original value.

### 3.3 Stray radiation

Unfortunately, an appreciable stray radiation problem was encountered during the first measurements on the spectrometer. The entrance waveguide was fed by means of a mode scrambler, resulting in a wide entrance pattern. Radiation was reflected by the upper half of the concave mirror directly into the lower exit waveguides, passing over the grating. This stray radiation amounted up to 7% of the maximum response of channel 1 and up to 2.5% for channel 6 (for a single frequency source! See Fig. 3.3.1). When a single mode was coupled into the entrance of the spectrometer, no stray radiation was seen.

It was considered that one cannot be sufficiently sure of the mode purity in the feeding waveguides from JET to omit measures against this phenomenon. Therefore, a "shielding wing" was constructed to shield the upper half of the concave mirror from the entrance slit. This reduced stray radiation even in the worst case (mode scrambler) to levels typically below 0.2% of peak values. However, this goes at the expense of channel 1 in particular, which is reduced to about 20% of its sensitivity. The other channels are affected as well, but not more than to about 80% of their sensitivity, depending on channel number; see Fig. 3.3.2. Moreover, this shielding wing tends to decrease the resolution of all channels because of unwanted reflections from the shielding wing into the exit waveguides. We have tried to overcome this problem by covering the wing with a special layer structure of thin eccosorb (Fig. 3.3.3). After the shielding wing was installed, the resolution is reduced to 85% of its value without the shielding wing fitted. This was considered acceptable because a more fundamental approach to the problem of stray radiation would incorporate a thorough change in the configuration of the spectrometer.

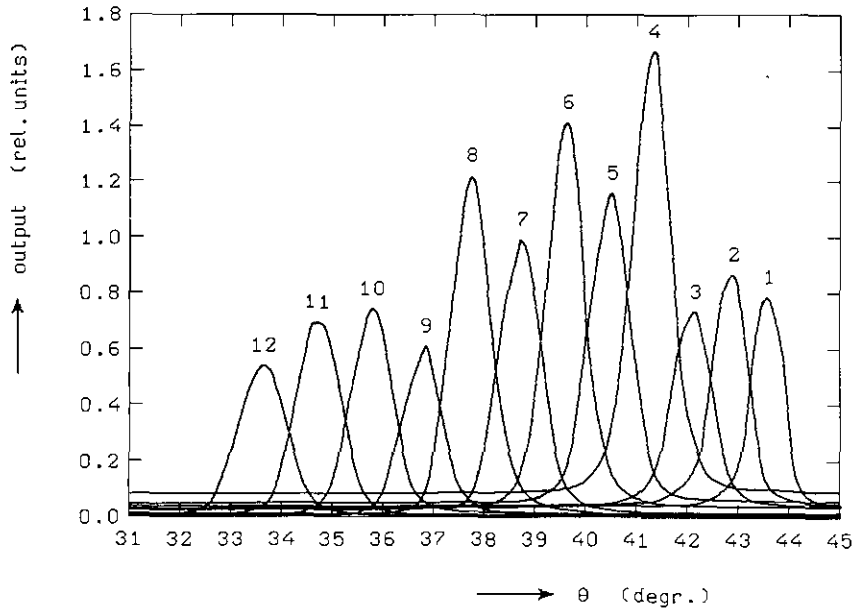


Fig. 3.3.1. A grating scan for  $f = 140$  GHz. The entrance waveguide is fed by means of a mode scrambler. Note the appreciable amount of stray radiation (7% for channel 1).

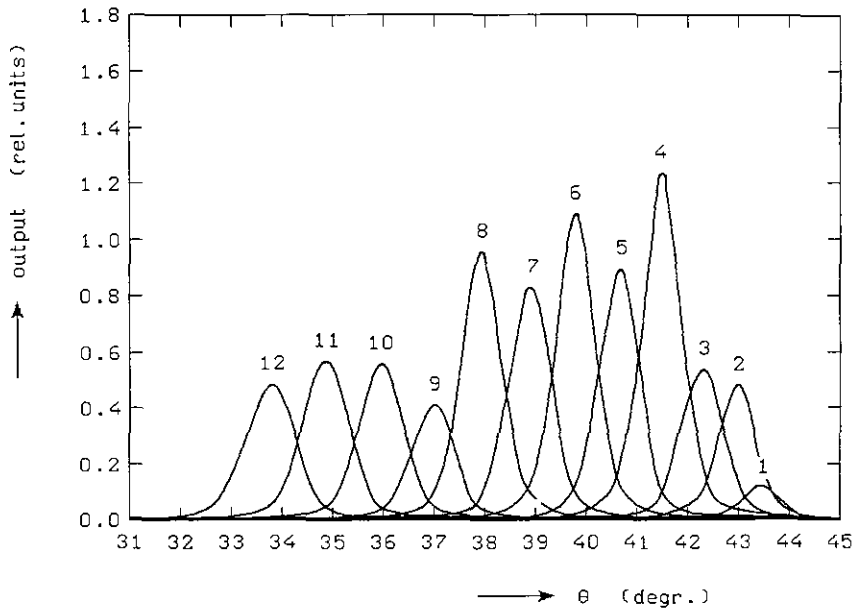


Fig. 3.3.2. The same measurement with the shielding wing fitted. The effect of stray radiation has been nullified.

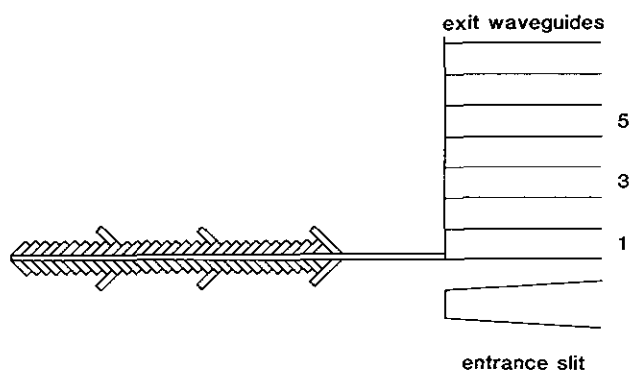


Fig. 3.3.3. A schematic view of the shielding wing as fitted into the spectrometer permanently.

### 3.4 Polarisation dependence

During the measurements it became clear that the grating efficiency for vertical polarisation ( $\underline{e}$  perpendicular to the grooves) exceeds that for the horizontal polarisation by about a factor of 10. This is in agreement with calculations based on the electromagnetic theory of gratings given in Ref. [7]. However, because of polarisation rotation in the entrance waveguide, the responsivity of the system is slightly better for horizontally polarised incoming radiation on the spectrometers entrance aperture with the preset angle  $\alpha_0$  of the entrance slit in the region of interest.

The amount of polarisation rotation has been measured. The BWO is used as a single mode frequency source, with known polarisation. With the use of a wire-grid polarisation filter placed directly after the entrance slit, the detector output of one channel is recorded as a function of the preset angle  $\alpha_0$ . This is done for both modes of incoming polarisation, see Fig. 3.4.1 and Fig. 3.4.2.

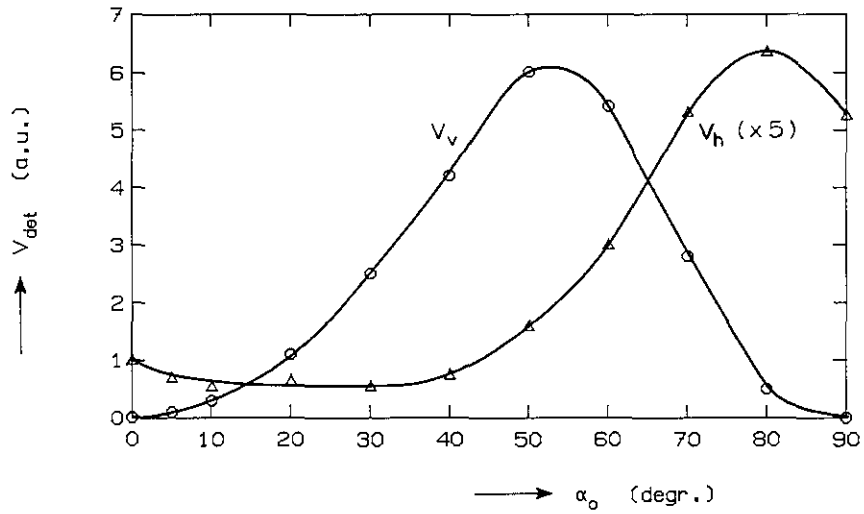


Fig. 3.4.1. Detector output as a function of a preset angle  $\alpha_0$ .  $V_v$  denotes detector output for vertical transmission,  $V_h$  for horizontal transmission. The incoming polarisation is horizontal.

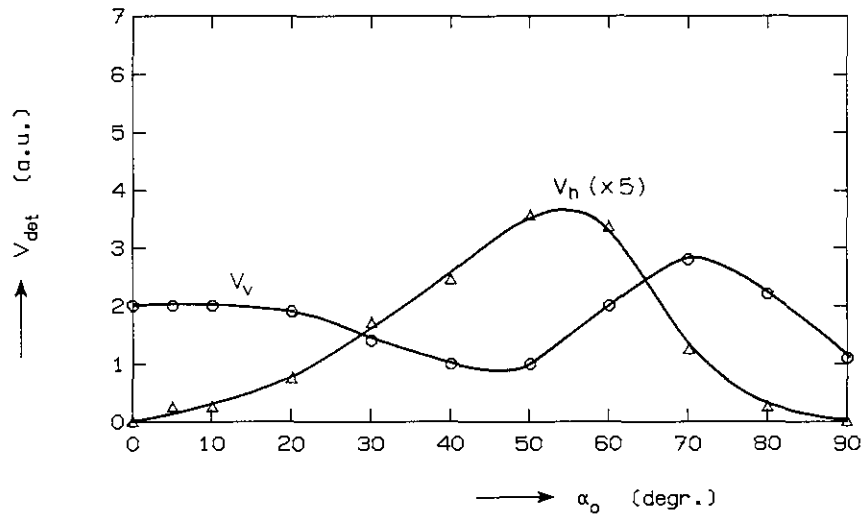


Fig. 3.4.2. The same nomenclature as in Fig. 3.4.1. The incoming polarisation is vertical.

From these measurements the rotation of the polarisation vector in the rotating section in the entrance waveguide can be calculated. Denoting  $V_v$  as the detector output when the polariser is set to transmit only vertical polarisation and  $V_h$  when only horizontal polarisation is transmitted, it follows from Fig. 3.4.3.:

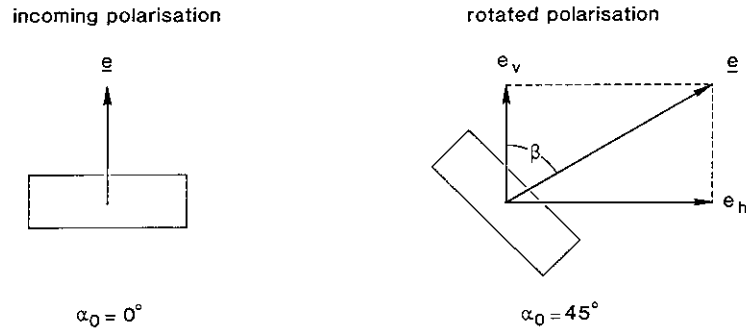


Fig. 3.4.3. Definition of the polarisation vector and its components when  $\underline{e}$  is rotated over an angle  $\beta$ .

$$\begin{aligned}
 v_v &\approx |e_v|^2 \\
 v_h &\approx \frac{1}{\eta} |e_h|^2
 \end{aligned}
 \tag{3.4.1}$$

With  $\eta$  the ratio of vertical to horizontal polarisation diffraction efficiencies ( $\eta = 10$ ). The rotation angle  $\beta$  of the polarisation vector can be calculated as:

$$\tan \beta = \left| \frac{e_h}{e_v} \right| = \left( \frac{v_h}{v_v} \eta \right)^{\frac{1}{2}}
 \tag{3.4.2}$$

A plot of  $\beta$  as a function of the preset angle  $\alpha_0$  is shown in Fig. 3.4.4.

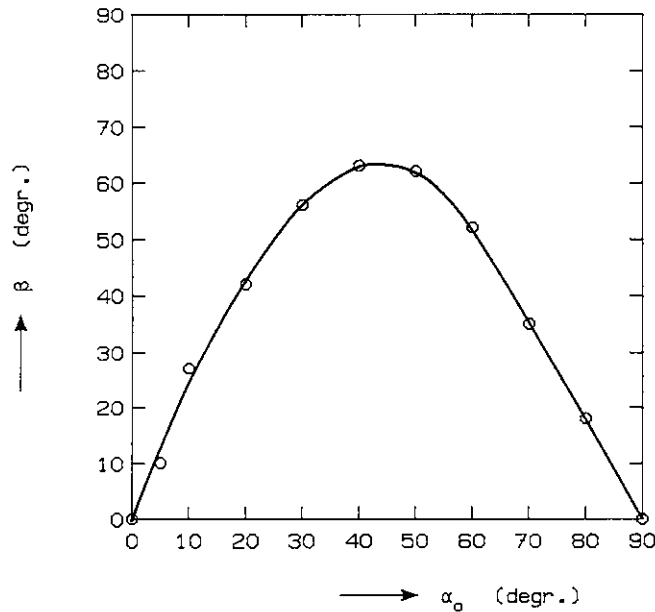


Fig. 3.4.4. The rotation angle  $\beta$  as a function of the preset angle  $\alpha_0$ .

From this figure it can be seen why the spectrometer gives more response for horizontal incoming polarisation. For the preset angles of interest ( $30^\circ < \alpha_0 < 70^\circ$ ) as much as 60 degrees rotation takes place, thereby gaining from the enhanced efficiency of the grating for the rotated electric field. It should be possible to enter the system with a tilted waveguide, thereby biasing the incoming polarisation. The extra rotation in the entrance waveguide then takes care that complete vertical polarised radiation falls on the grating. Of course, this situation can only be achieved for one particular preset angle. It can be calculated that the signal gain can be more than 40%, depending on frequency (grating angle) and desired resolution.

### 3.5 Different entrance slits

Some experiments were performed using different dimensions of the entrance slit. In first instance, a  $40.0 \times 7.0$  mm entrance slit was mounted in the spectrometer. As the exit waveguides measure  $40.0 \times 13.5$  mm and both entrance and exit waveguides are in the focal plane of the concave mirror, it was thought that by enlarging the smaller dimension of the entrance slit, some gain in sensitivity can be reached without affecting the resolution too much. The starting point is the fact that the deformation of the spectral image is corrected by presetting  $\alpha_0$ . Then three different entrance slits were mounted in the spectrometer and the resolution as well as the multi-mode response for each of them were measured. The multi-mode measurements were performed with the aid of a calibration rig (described in Section 4.1) and by calculating the response of the system from an integration of the antenna pattern (the method is described in Ref. [8]).

The results are presented in Table 3.5.1. As can be seen, replacing the 7 mm entrance by a 13.5 mm slit only slightly deteriorated the resolution. The responsivity of the system increased by about 70% (as an average for both polarisations). Using 20 mm entrance slit again increases the responsivity by another 45%, however the resolution decreases by roughly the same factor. All measurements were done at a frequency of 140 GHz and were performed on channel 7; the shielding wing was not fitted in this case.

TABLE 3.5.1.

Entrance slit	Vertical Pol.		Horizontal Pol.	
	Relative response	resol.	Relative response	resol.
40.0 × 7.0 mm	1.00	96	1.00	100
40.0 × 13.5 mm	1.60	92	1.79	85
40.0 × 20.0 mm	2.47	56	2.48	58

As a result of this measurement, an entrance slit of 40.0×13.5 mm has been installed in the spectrometer permanently.

#### 4. ANTENNA PATTERN MEASUREMENTS

##### 4.1 Introduction

Antenna pattern measurements were performed to obtain information on the responsivities, mode contents and attenuation of different components of the spectrometer. To do this kind of measurement properly, a special calibration rig has been constructed. It consists of two beams of which each of them can be rotated around a central axis independently. The receiving antenna (or waveguide aperture) is placed at the intersection point of these virtual axis. The advantage of this configuration is that the frequency source (or a detector) is always pointed to the origin of the waveguide aperture, irrespective of the angular position of the source. Both beams are rotated by stepping motors and harmonic drives give the necessary gear reduction and torque multiplication. The drivers of the stepping motors are interfaced with the PDP 11/23 computer; in this way fully automated antenna patterns scans can be made. The detector output voltage is stored in a data file for each position of the source, which makes it possible to integrate the antenna patterns numerically. The calibration rig is shown as a schematic view in Fig. 4.1.1.

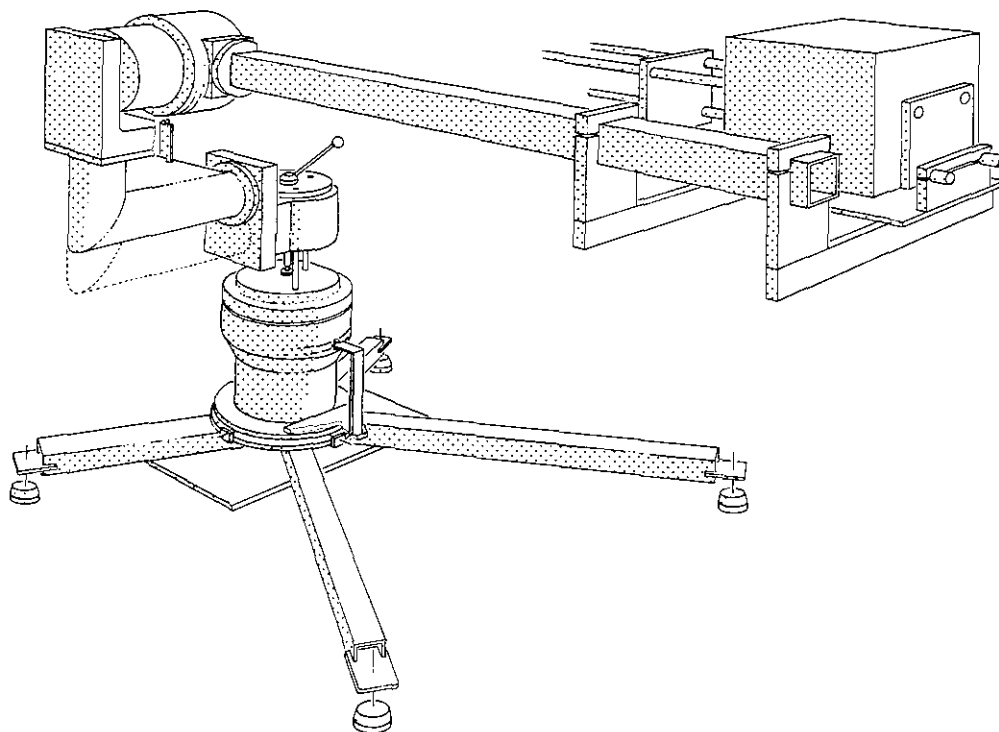


Fig. 4.1.1. Schematic view of the calibration rig. The two large cylinders contain the stepping motors and harmonic drives; the height is adjustable. This configuration ensures the source (BWO) to be pointing to the origin of the waveguide aperture.

The attenuation of a component of the spectrometer is defined as the ratio of the 2-dimensional integral of the pattern as measured before and after this component is inserted in the system. The number of modes in the pattern are calculated with the formula:

$$N = \frac{A\Omega}{\lambda^2} , \quad (4.1.1)$$

with N the approximate number of modes,  
A the area of the antenna aperture,  
 $\Omega$  the 1/e width of the solid angle of the pattern,  
 $\lambda$  the wavelength.

#### 4.2 Patterns of several components

A contour plot of the antenna pattern of the detector of channel 5 of the spectrometer is shown in Fig. 4.2.1. Radiation is transported to the detector by means of a 15 cm long circular waveguide ( $\emptyset$  15 mm) mounted in the cryostat bottom. The radiation is then collected with a f2-Winston cone, tapering to the cavity where the detector chip is mounted in. The frequency used is  $f = 140$  GHz and the incoming polarisation is vertical. The E-plane and H-plane of the pattern are shown in Figs. 4.2.2 and 4.2.3. From Eq. 4.1.1 it can be calculated that the approximate number of modes contained in the pattern is 20. Because of the error introduced when determining  $\Omega$  (about 20% error), this is only a global figure. It is thought that this pattern is too broad for our applications because the mode-selective grating of the spectrometer limits the number of modes to about 2.5 at  $f = 140$  GHz. Therefore it is desirable to narrow down the pattern and, at the same time, increase the single mode response. An attempt was made to improve the single mode response by changing the focussing optics of the detectors. Until now an increase of a factor 2 has been achieved by inserting a lens (focussing on the detector-chip) in the cryostat bottom.

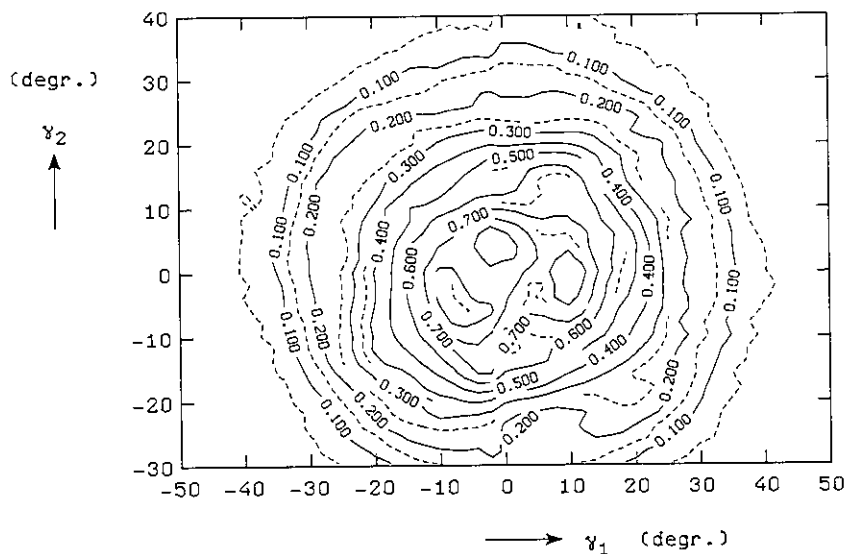


Fig. 4.2.1. Contour plot of the antenna pattern measured in front of the detector of channel 5. The incoming polarisation is vertical: E-plane corresponds to the  $(0, \gamma_2)$  plane, H-plane corresponds to the  $(\gamma_1, 0)$  plane.

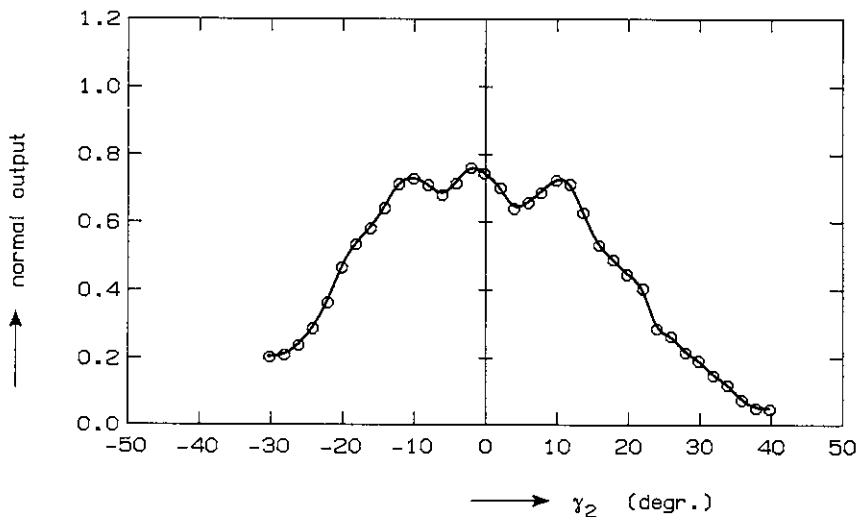


Fig. 4.2.2. E-plane of the detector antenna pattern.

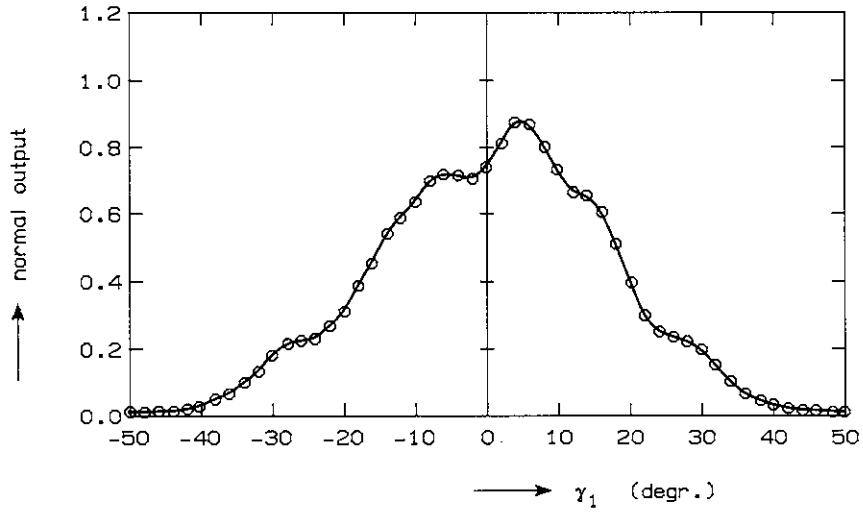


Fig. 4.2.3. H-plane of the detector antenna pattern.

The Figs. 4.2.4 and 4.2.5 show E- and H-plane scans of the rectangular to circular mode converter linked to the piece of circular waveguide. Because no complete scan has been made, a contour plot is not available. The approximate number of modes is 24, as calculated with Eq. 4.1.1.

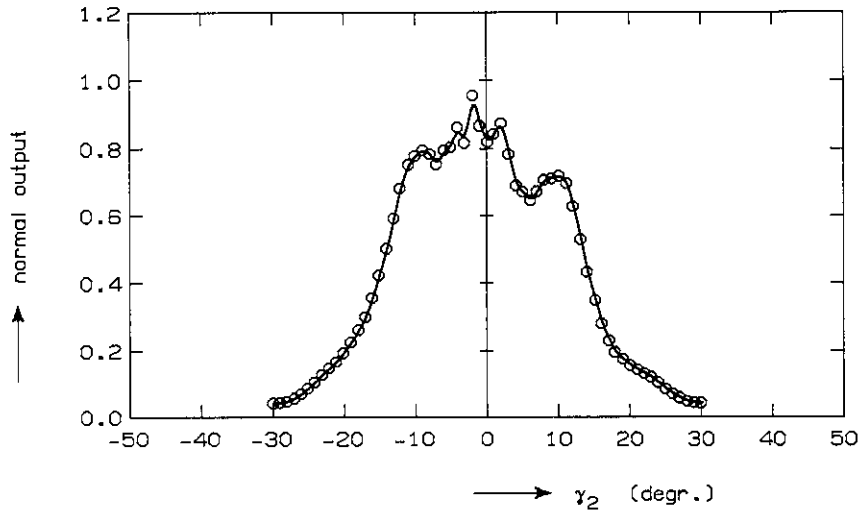


Fig. 4.2.4. E-plane of the antenna pattern with the rectangular to circular mode converter linked to the cryostat bottom.

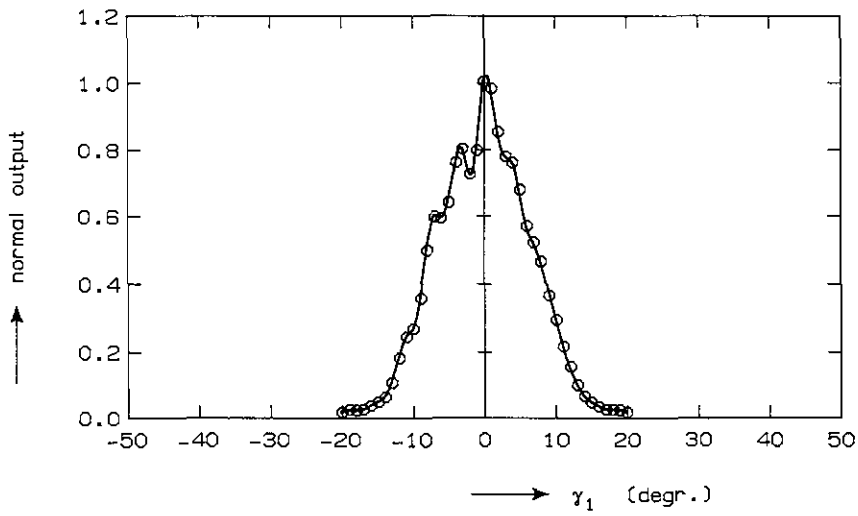


Fig. 4.2.5. Ibidem, H-plane.

The antenna pattern made in front of the exit waveguide of channel 5 is given in Figs. 4.2.6 - 4.2.8. The number of modes is still 17. The attenuation of the exit waveguide plus mode converter amounts to 3.5 dB.

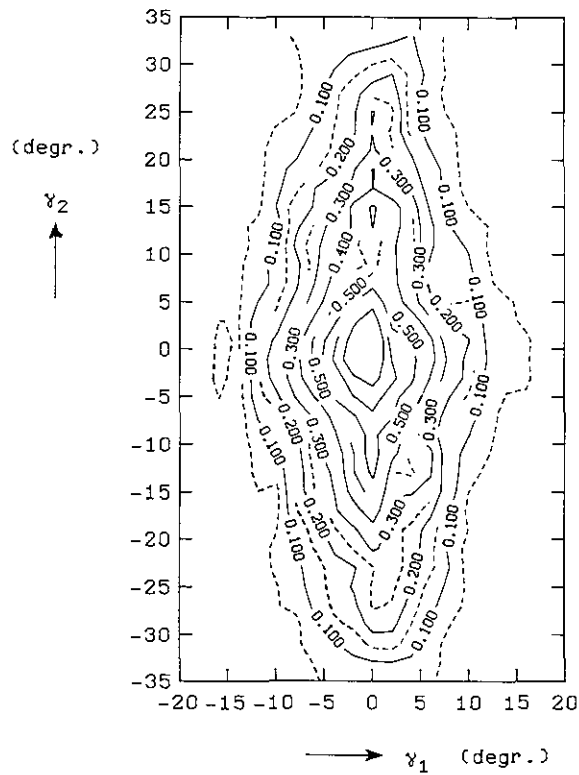


Fig. 4.2.6. Contour plot of the antenna pattern measured in front of the exit exit waveguide of channel 5. The incoming polarisation is vertical.

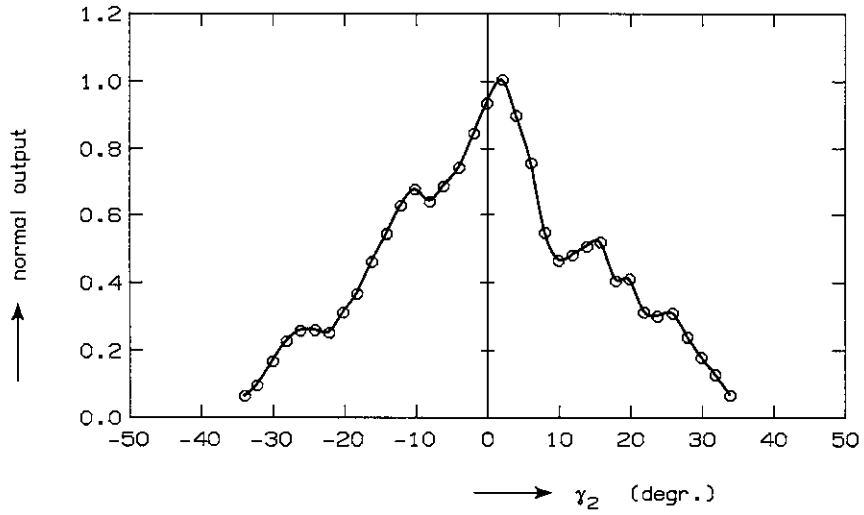


Fig. 4.2.7. E-plane of the exit waveguide antenna pattern.

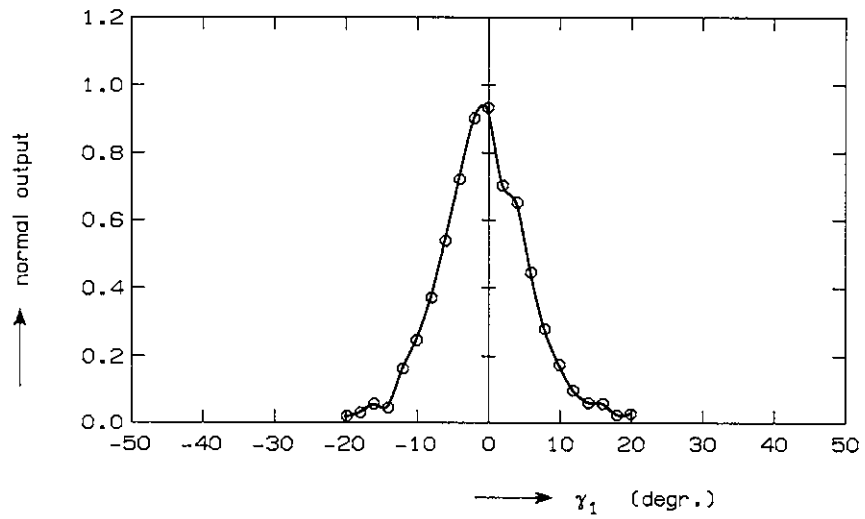


Fig. 4.2.8. H-plane of the exit waveguide antenna pattern.

Finally, the E-and H-planes of the pattern made in front of the system's entrance are shown in Figs. 4.2.9 and 4.2.10. the number of modes has now reduced to 2.5; total attenuation amounts to 15 dB for the multi-mode case. The response in terms of  $eV/\mu V$  (Ref. [8]) for all components described is given in Table 4.2.1. The antenna patterns and responsivities measured at the beginning of the JET waveguide will be reported later.

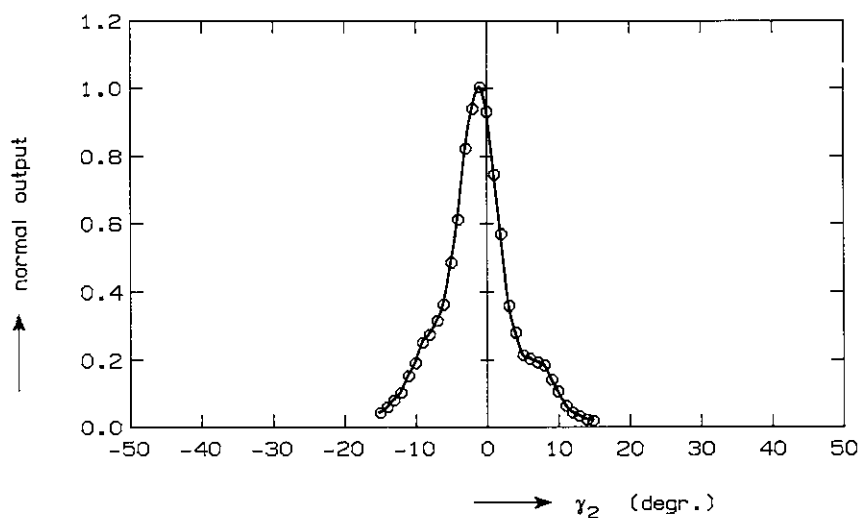


Fig. 4.2.9. E-plane of the antenna pattern measured in front of the system's entrance. The spectrometer is tuned for channel 5 to receive  $f = 140$  GHz radiation.

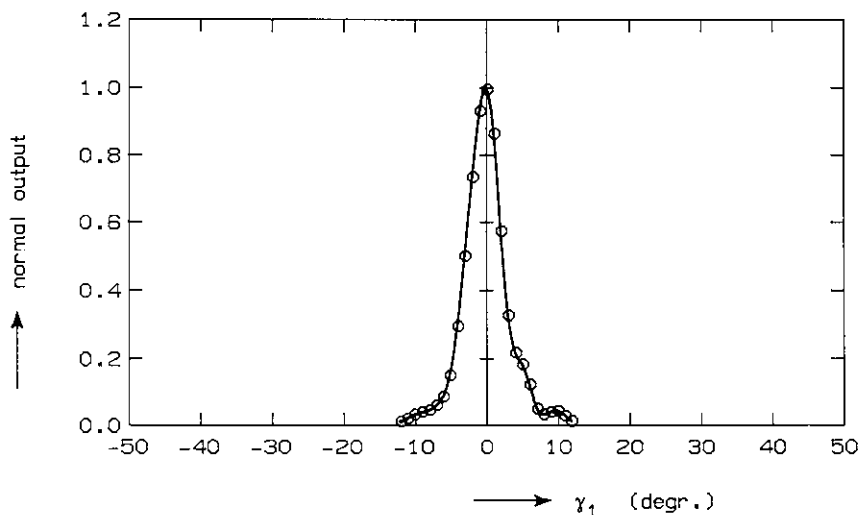


Fig. 4.2.10. Ibidem, H-plane.

TABLE 4.2.1

location of measurement	Responsiv. (eV/ $\mu$ V)	N modes	attenuation
at cryostat window	0.20	20	} 3.5 dB
at exit waveguide	0.45	17	
at system's entrance	7.7	2.5	} 12 dB

NOTE: The response is given in eV/ $\mu$ V; in fact this figure is related to the black body temperature needed to obtain 1  $\mu$ V detector output. Frequency 140 GHz.

## 5. ABSOLUTE CALIBRATION OF THE POLYCHROMATOR

### 5.1 Introduction

There exists several techniques to perform an absolute calibration of a grating polychromator. A method commonly used to calibrate ECE spectrometers (e.g. Michelson interferometers) is using a large area black body source of well-known temperature placed in front of the waveguide system leading to the spectrometer. Another method is deriving calibration data from an already calibrated diagnostic, e.g. a calibrated Michelson interferometer or Thomson scattering. A third one comprises the use of a microwave source scanning in front of the waveguide system and integrating the antenna pattern. Another possible technique is the use of a microwave source in combination with a mode scrambler. These four methods will be described separately.

### 5.2 Large area black body source

The calibration with a large area black body is routinely performed for calibrating the ECE Michelson interferometer at JET [9]. In this technique, a large area source of known temperature and emissivity fills the antenna pattern. Interferograms are coherently added to enhance the signal to noise ratio (signal averaging). The main advantage of this technique is the high frequency range (100-1000 GHz) of the black body source and the straightforward conversion of black body source temperature to detector output voltage. This method is, however, less suitable for grating polychromators because of the relatively low temperature of the source (400 K). Because of the resulting low signal levels, integration times of about one hour for each of the twelve channels and for each selected frequency will be necessary. This results in a total calibration time of more than 300 hours if 25 frequencies are monitored and only one signal averager is available. To test the method, a set-up was made with the hot source in front of a piece of waveguide containing two low-pass unidirectional grating filters (205 GHz and 250 GHz cutoff) and a polarisor to select the horizontal polarisation mode.

The grating was set for channel 5 to receive  $f = 140$  GHz radiation. The responsivity derived from this method of calibration is  $R_V = 6.5$  eV/ $\mu$ V for the source at system entrance.

### 5.3 Cross-calibration

The method of cross-calibration against an already calibrated diagnostic is of course a trivial one. The detector output voltage of a channel tuned to a certain frequency is averaged over a certain time interval during a JET discharge and compared to the plasma temperature as derived from a Michelson interferometer for that frequency. The advantage of this method is that for each JET pulse calibration data are obtained. The main disadvantage is that in fact the same temperature profiles as inferred from the Michelson are measured, albeit on a much faster time scale. A responsivity characteristic of channel 5 obtained by this method of calibration is shown in Fig. 5.3.1. The curve is fitted through datapoints inferred from 10 JET discharges. Note that the complete waveguide system JET-spectrometer is included in this calibration. Therefore, a factor of  $\pm 17$  is lost in the waveguides.

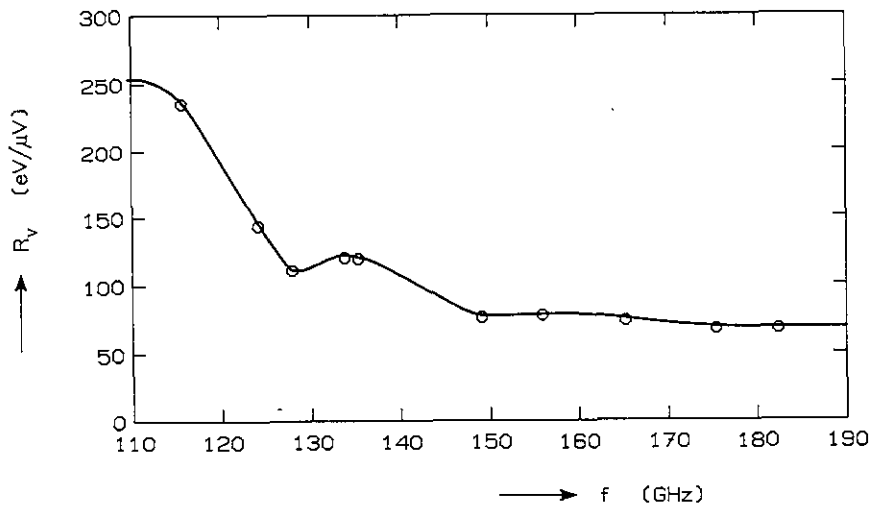


Fig. 5.3.1. The responsivity of the spectrometer obtained by cross-calibration against a Michelson interferometer. The waveguide system is thus included.

### 5.4 Antenna pattern integrations

The method of deriving calibration factors from an antenna pattern integration is fully described in Ref. [8]. It is shown that a large area black body can be simulated by a two-dimensional scan of a microwave source. Either a single frequency or a sweeping microwave source can be used. With a single frequency source the bandwidth of the system is still unknown and has to be determined separately. When a sweeping source is employed, the systems bandwidth is included in the calibration. The responsivity in terms of eV/μV is then given by:

$$R_v = \frac{G P_s c^2}{4 \pi Q_v f^2 \Delta f e}, \quad (5.4.1)$$

with:

G the antenna gain of the source

$P_s$  the power of the source in  $\mu W$

$Q_v$  the integral of the pattern in  $Vm^2$

f the frequency of the source

$\Delta f$  the system's bandwidth or the sweepwidth of the source (exceeding the system's bandwidth).

The advantage of this method of calibration is that, as long as the two-dimensional scan entirely covers the antenna pattern of the system, it can be very accurate. However, the accuracy of the method crucially depends on the knowledge of  $P_s$ ; a reliable standard to determine this power is required. A disadvantage is the considerable amount of work going into the calibration of the 12-channel polychromator for 25 different frequencies. Total estimated calibration time would yield about 300 hours.

### 5.5 Mode scrambler

This method of calibration uses a single frequency source (BWO) and a mode scrambler stirring up the single input mode. The mode scrambler has two exit apertures: one tapering down to fundamental waveguide to allow for power measurements, the other smoothly tapering up to the dimensions of the receiving antenna or waveguide aperture which leads to the spectrometer. The whole set-up is in fact a closed system. This calibration method is only valid when two conditions are fulfilled:

- The number of modes generated in the mode scrambler must exceed the number of modes accepted by the spectrometer/detector.
- No mode conversion into high order modes which will not be detected is allowed between mode scrambler and detector. Because all modes are excited in the system with power  $kT\Delta f$  in the frequency band  $\Delta f$  of interest, mode conversion will not change the total power. However, mode conversion of low order modes which could be detected into high order modes that are either reflected somewhere or are not accepted by the detector will degrade the transmission of the system.

The fundamental input power from the source will be evenly distributed over all modes generated in the mode scrambler:

$$P_s = N k T_{eq} \Delta f \quad (5.5.1)$$

with  $P_s$  the power from the source  
 $N$  the number of modes  
 $T_{eq}$  some equivalent temperature  
 $\Delta f$  the bandwidth of the system.

In this way, a black body of temperature  $T_{eq}$  can be simulated provided that  $N$  is sufficiently large (compared to the number of modes accepted by the system). The responsivity of the system defined as the constant of proportionality between the black body temperature in electronvolt and the detector output voltage in microvolt can be written as:

$$R_v = \frac{k T_{eq}}{e V_{det}} = \frac{P_s}{N e V_{det} \Delta f} \quad [eV/\mu V]$$

with  $e$  the elementary charge.

Inserting  $N = 1$  yields:

$$R_v = \frac{P_{fun}}{e V_{det} \Delta f} \quad (5.5.2)$$

with  $P_{fun}$  the power in one single, fundamental mode. Because  $\Delta f$  is unknown,  $V_{det} \Delta f$  can be replaced by:

$$V_{det} \Delta f = \int_{f_{min}}^{f_{max}} V_{det} df = \int_{\vartheta_{min}}^{\vartheta_{max}} V_{det} \frac{\partial f}{\partial \vartheta} d\vartheta, \quad (5.5.3)$$

with  $\vartheta$  the grating angle. The values of  $\vartheta_{min}$  and  $\vartheta_{max}$  have to be taken in such a way in order to satisfy:

$$\begin{aligned} V_{det} &= 0 \text{ for } \vartheta < \vartheta_{min} \text{ and } \vartheta > \vartheta_{max}. \\ V_{det} &\neq 0 \text{ for } \vartheta_{min} < \vartheta < \vartheta_{max}. \end{aligned}$$

The variation of frequency with the grating angle,  $\partial f/\partial \vartheta$ , is known from the dispersion curves (Sect. 3.1).

Combining (5.5.2) and (5.5.3) results in:

$$R_V = \frac{P_{fun}}{e \int_{\vartheta_{min}}^{\vartheta_{max}} V_{det} \frac{\partial f}{\partial \vartheta} d\vartheta} \quad [eV/\mu V] \quad . \quad (5.5.4)$$

The power in the fundamental mode  $P_{fun}$  is measured with a power meter coupled to the fundamental exit aperture of the mode scrambler. For a single frequency, the grating is rotated between  $\vartheta_{min}$  and  $\vartheta_{max}$ , as described in Sect. 3.1.

This kind of measurement is also used to determine the relative responsivities of all twelve channels of the spectrometer (i.e. relative to one channel). The power in the fundamental mode is then not of interest provided it remains constant during the measurements.

The main advantage of this method of calibration is that it is fast: all twelve channels can be monitored for one frequency in about 40 minutes. Total calibration time for 25 different frequencies would be approximately 17 hours. Disadvantages are the need for an exact power- measurement (within 10% error) of the fundamental mode power extracted from the mode scrambler and the fact that there will always be a (modest) amount of mode conversion from modes which would originally be seen by the detector into modes which are not accepted. This latter phenomenon will result in a measured responsivity which is lower than the actual responsivity.

## 6. CONCLUSIONS AND DISCUSSION

The 12-channel grating polychromator has proved to be an adequate ECE-diagnostic for electron temperature measurements as can be inferred from the first results obtained at JET. The problem of stray radiation has been overcome by fitting a shielding wing. However, this comes at the expense of some loss in responsivity and resolution. Improvements in the system's response have been made by inserting a focussing lens in the cryostat bottom and by optimising the dimensions of the entrance aperture. A more substantial improvement could be obtained by narrowing down the detectors antenna pattern and, at the same time, increasing the single mode response. This aspect is still under investigation.

The rotation of the polarisation vector in the rotating section of the entrance waveguide gives rise to a loss in responsivity because of the large difference in grating efficiencies to horizontal and vertical polarisation. This problem has been dealt with by changing the incoming polarisation at system entrance from vertical to horizontal. To gain more response by biasing the incoming polarisation vector by means of a tilted waveguide would be possible.

The method of absolute calibration of all 12 channels of the spectrometer has still to be decided upon. The use of a large area black body source is still favourable, but this would take too long a calibration time. A cross-calibration against a Michelson interferometer is, of course, the fastest and most simple way, but has the disadvantage of being dependent on another diagnostic.

A comparison of the three different methods for calibrating ECE systems (hot source, antenna pattern scan and mode scrambler) will be performed and the results will be presented shortly [10].

First measurements on a rapid-scan Michelson interferometer indicate a coherence between the three methods within 30%.

It is obvious that when these measurements justify the use of the mode scrambler as a calibration source, this method is favourable because of the short calibration time.

REFERENCES

1. Piekaar, H.W. and Rutgers, W.R., "A diagnostic design study for ECE-measurements on the Joint European Torus using a grating polychromator", JET contract No. 19.2; Internal Report Rijnhuizen I.R. 80/007, Nieuwegein, The Netherlands (1980).
2. Bornatici, M., Cano, R., De Barbieri, O. and Engelmann, F., "Electron cyclotron emission and absorption in fusion plasmas", Nucl. Fusion 23 (1983) 1153.
3. Sillen, R.M.J., Piekaar, H.W. and Oyevaar, Th., "A FIR grating polychromator using conical diffraction as a diagnostic tool for ECE plasma measurements", Infrared Phys. 24 (1984) 511.
4. Barbian, E.P. and De Zwart, G.W., "Reflective filters for ECE measurements", to be published.
5. Timusk, T. and Richards, P.L., Appl. Opt. 20 (1981) 1355.
6. Tubbing, B.J.D., "Design and construction of a mode converter from  $TE_{10}$  to  $TE_{11}$ ", Rijnhuizen Report 84-158, Nieuwegein, The Netherlands (1984).
7. Petit, R. et al., "Electromagnetic theory of gratings", Springer Verlag Berlin, Heidelberg, New York (1980).
8. Tubbing, B.J.D., "An absolute calibration method for electron cyclotron emission spectrometers", Rijnhuizen Report 83-149, Nieuwegein, The Netherlands (1983).
9. Baker, E.A.M. et al., "Absolute calibration of the JET ECE system", 4th Int. Workshop on ECE and ECRH, Frascati, March 1984.
10. Baker, E.A.M. et al., "A comparison of three different methods for calibrating ECE measurement systems", Proc. EC5, 5th Int. Workshop on Electron Cyclotron Emission and Electron Cyclotron Heating, San Diego, 9-12 November 1985.